Trimetallic Hydrotreating Catalysts $CoMoW/Al_2O_3$ and $NiMoW/Al_2O_3$ Prepared on the Basis of Mixed Mo-W Heteropolyacid: Difference in Synergistic Effects

A. V. Mozhaev[a], M. S. Nikul'shina[a, b], C. Lancelot[b], P. Blanchard[b], C. Lamonier[b], and P. A. Nikul'shin[a, c, *]

[a] *Samara State Technical University, Samara, 443100 Russia*

[b] *Université Lille1, UCCS, Cité Scientifique, Bât. C3 59655, Villeneuve d'Ascq, France*

[c] *All-Russia Research Institute of Oil Refining, Moscow, 111116 Russia*

**e-mail: p.a.nikulshin@gmail.com*

Received August 2, 2018

Abstract—Trimetallic $CoMo_3W_9/Al_2O_3$ catalyst is prepared using the Keggin structure mixed heteropolyacid $H_4SiMo_3W_9O_{40}$ and cobalt citrate. $CoMo_{12}/Al_2O_3$ and CoW_{12}/Al_2O_3 catalysts based on $H_4SiMo_{12}O_{40}$ and $H_4SiW_{12}O_{40}$, respectively, are synthesized as reference samples. Sulfided catalysts are analyzed by high-resolution transmission electron microscopy and X-ray photoelectron spectroscopy. Catalytic properties are investigated in the co-hydrotreatment of dibenzothiophene (DBT) and naphthalene in a flow unit. It is shown that the catalytic activity in both DBT hydrodesulfurization and naphthalene hydrogenation (HYD) decreases in the following sequence: $CoMo_{12}/Al_2O_3 > CoMo_3W_9/Al_2O_3 > CoW_{12}/Al_2O_3$, and it correlates with the degree of promotion of active-phase particles by cobalt atoms. A comparison with the published data available for Ni-promoted catalysts makes it possible to reveal the general regularity for bi- and trimetallic Co(Ni)-Mo(W)S catalysts: the use of mixed Mo-W $H_4SiMo_3W_9O_{40}$ heteropolyacid instead of monometallic $H_4SiW_{12}O_{40}$ causes an increase in the degree of promotion of $MoWS_2$ crystallite edges for the series of catalysts promoted by both cobalt and nickel. The use of nickel as a promoter leads to a higher degree of promotion of edges of active-phase particles in comparison with cobalt; as a result, the $NiMo_3W_9/Al_2O_3$ catalyst is much more active than the $CoMo_3W_9/Al_2O_3$ counterpart. Possible reasons behind the found features are discussed.

Keywords: hydrotreating, CoMoWS, NiMoWS, dibenzothiophene, naphthalene

DOI: 10.1134/S0965544118140104

A deep hydrotreating of hydrocarbon feedstock becomes all the more urgent in connection with the need to produce environmentally friendly fuels from heavy oil fractions and residues and because of the involvement of high-sulfur oils in refining. Therefore, the design of new catalytic materials is aimed at increasing their hydrogenation activity necessary to improve the energy efficiency of hydrocatalytic processes owing to reduction in operational costs. $Co(Ni)Mo(W)/Al_2O_3$ catalysts have been used in hydrogenation processes for more than eight decades [1–3]. The active phase in these catalysts is Co(Ni)Mo(W)S-type structures which are formed during catalyst activation (sulfiding); these are nanosized MoS_2 or WS_2 crystallites decorated by Co and/or Ni promoter atoms at the edges [4].

Catalysts based on WS_2 feature as a rule high activity in hydrogenation reactions and possess an increased stability [5]. The improvement of promoted Co(Ni)W catalyst systems is at the focus of ever growing attention [6, 7]. Previous studies showed that Co(Ni)Mo catalysts exhibit a higher catalytic activity in hydrodesulfurization (HDS) reactions compared with their Co(Ni)W analogs [3, 8–12]. In accordance with Vissenberg et al. [13], one of the reasons behind a low HDS activity of Co(Ni)W catalysts is a great difference in sulfiding conditions for supported oxide precursors, in particular, overly high sulfiding temperatures for W oxides compared with Co or Ni oxides. Therefore, during activation of Co(Ni)W catalysts, the sulfiding of Co(Ni) promoter atoms occurs initially to generate CoS_x (NiS_x) massive variable-composition sulfides inactive in catalysis and only then are WS_2 crystallites formed. Nevertheless, the authors of [13, 14] disclosed a high promoting effect of Ni related to the post-formation of NiWS sites via the redistribution of NiS_x particles, namely, the migration of a portion of promoter atoms and their localization at tungsten sulfide edges [13, 14]. Much less data are available on CoW catalysts, although attempts to gain insight

Table 1. Composition and textural characteristics of $CoMo(W)/Al_2O_3$ catalysts

Catalyst	Content, wt %			Textural characteristics of sulfide samples		
	MoO_3	WO_3	CoO	surface area S_{BET}, m^2/g	pore volume V_p, cm^3/g	pore diameter, nm
$CoMo_{12}/Al_2O_3$	18.0	–	4.7	291	0.55	3.8/8.4
CoW_{12}/Al_2O_3	–	26.2	4.2	265	0.50	3.8/8.4
$CoMo_3W_9/Al_2O_3$	4.2	20.1	4.3	288	0.56	3.8/8.4

into causes of their low catalytic activity and to eliminate them to date do not cease [15–17].

One of the known methods to increase the activity of hydrotreating catalysts involves the incorporation of complexing agents into their composition [18–20]. Owing to the formation of stable complexes with Ni (Co), the use of chelatons makes it possible to decelerate the preliminary sulfiding of promoters or to synchronize it with the sulfiding of main metals (Mo and W). As a result, selectivity for formation Co(Ni)Mo(W)S active-phase particles grows.

Another method to enhance catalyst activity in HDS and HYD reactions includes the application of trimetallic Ni(Co)MoWS catalysts, in which a portion of tungsten atoms is replaced with molybdenum or vice versa [21–26]. The feasible synergistic effect in the co-use of Ni, Mo, and W was predicted by the density function theory (DFT) [23, 27]. As was shown in [1, 28, 29], the use of the Keggin structure mixed Mo-W heteropolycompounds as precursors of MoW/Al_2O_3 and $NiMoW/Al_2O_3$ hydrotreating catalysts, in which one or three W atoms of the 12 are replaced with Mo, ensures the spatial proximity of Mo and W atoms. This enables preparation of the mixed $MoWS_2$ phase; its composition and structure are ascertained using a scanning transmission electron microscope and a high-angle annular dark field (HAADF) detector. Given this, the degree of sulfiding tungsten grows and, as a consequence, the amount of active-phase particles increases appreciably. Moreover, the degree of promotion of active-phase edge sites by nickel on the NiMoW catalyst is ~30% higher than that on the NiW/Al_2O_3 catalyst [1]. Trimetallic CoMoWS hydrotreating catalysts are attracting all the more growing attention from researchers [15, 26, 30, 31], although the data on their activity are ambiguous. For example, in accordance with [17, 30], massive NiMoWS catalysts are much more active than CoMoWS analogs. However, as was reported recently by Pawelec et al. [15], owing to increased acidity (due to the partial replacement of Mo atoms with W ones), the $CoMoW/Al_2O_3$-TiO_2 catalyst shows a considerably higher activity in the hydrodesulfurization of DBT; this parameter is even higher than the activity of the $CoMo/Al_2O_3$ commercial reference sample.

The aim of this work was to explore the effect of Co promotion for the $CoMoW/Al_2O_3$ trimetallic catalyst. For this purpose, catalysts were synthesized using mixed $H_4SiMo_3W_9O_{40}$ heteropolyacid (HPA) and cobalt citrate as precursors of the active phase and bimetallic $CoMo/Al_2O_3$ and CoW/Al_2O_3 reference samples on the basis of corresponding monometallic $H_4SiMo_{12}O_{40}$ ($SiMo_{12}$HPA) and $H_4SiW_{12}O_{40}$ (SiW_{12}HPA) HPAs. The synthesized catalysts in the activated (sulfide) state were studied by high-resolution transmission electron microscopy (HRTEM) and X-ray photoelectron spectroscopy (XPS). Using these methods, the composition and structure of active-phase nanosized particles were ascertained and the catalytic behavior of the catalysts in dibenzothiophene HDS and naphthalene HYD model reactions was explored.

EXPERIMENTAL

Precursors of the active phase of catalysts were Keggin structure heteropolyacids. Monometallic $H_4SiMo_{12}O_{40}$ and $H_4SiW_{12}O_{40}$ and mixed $H_4[SiMo_3W_9O_{40}]$ HPAs were synthesized as described in [32–34]. The composition and structure of HPAs were studied by IR and Raman spectroscopy, X-ray diffraction, and EXAFS.

$CoMo/Al_2O_3$, CoW/Al_2O_3, and $CoMo_3W_9/Al_2O_3$ catalysts with the same surface loading of metals Mo + W ~ 4 at/nm^2 were prepared by the single incipient wetness impregnation of the support (specific surface area, 275 m^2/g; specific pore volume, 0.9 cm^3/g) with the aqueous solution of corresponding HPAs and cobalt citrate. After impregnation, the samples were dried at 110°C. The content of metals in the catalysts was monitored using an EDX800HS X-ray fluorescence analyzer (Shimadzu). The compositions of the synthesized catalysts are presented in Table 1.

The textural characteristics of the catalyst samples were investigated by low-temperature nitrogen adsorption on a Quantachrome Autosorb-1 adsorption porosimeter. The specific surface area was calculated according to the Brunauer–Emmett–Teller (BET) model for $P/P_0 = 0.05–0.3$. The total pore volume and pore size distribution were calculated from

the desorption curve in terms of the Barrett–Joyner–Halenda model.

The XPS studies of sulfide catalysts were conducted on a Kratos Axis Ultra DLD spectrometer using AlK_α radiation ($h\nu$ = 1486.6 eV). The binding energy (E_b) scale was preliminarily calibrated against position of the peaks of core levels $Au4f_{7/2}$ (84.0 eV) and $Cu2p_{3/2}$ (932.67 eV). The samples were applied on a double-sided nonconducting adhesive tape. The charging effect arising during the photoemission of electrons was minimized through irradiation of the sample surface by low-energy electrons of a special source (flood gun). Calibration was made against the C1*s* line (284.8 eV) of carbon occurring on the surface of the catalyst. The energy step was 1 eV for the survey spectrum and 0.1 eV for individual lines C1*s*, Al2*p*, S2*p*, Mo3*d*, and W4*f*. The decomposition of the Mo3*d* and W4*f* lines was conducted in accordance with parameters described in [35–37]. For all sulfide catalysts, the relative concentrations of W^{6+} (Mo^{6+}) and Co^{2+} particles in the oxide environment, oxysulfides WS_xO_y (MoS_xO_y), and sulfides WS_2 (MoS_2), CoW(Mo)S, Co_9S_8 were determined. For example, the relative concentration of WS_2 particles was calculated through the following equation:

$$[WS_2](\%) = \frac{A_{WS_2}}{A_{WS_2} + A_{WS_xO_y} + A_{W^{6+}}} \times 100, \qquad (1)$$

where A_X is the area under the peak of particles x.

The amount of cobalt in the Co(Mo)WS phase was determined via the following equation:

$$c_{Co(Mo)WS} = [CoMo(W)S]c_{Co}, \qquad (2)$$

where C_{Co} is the total content of Co measured using XPS, wt %.

The degree of promotion of active-phase crystallites was calculated by the following equation:

$$\left(\frac{Co}{Mo + W}\right)_{slab} = \frac{c_{Co(Mo)WS}}{c_{W(Mo)S_2}}, \qquad (3)$$

where C_X is the absolute concentration of Co(Mo + W) in Co(Mo)WS particles, at %.

The degree of promotion of the edges of active-phase crystallites was determined in accordance with [37] through the following equation:

$$\left(\frac{Co}{Mo + W}\right)_{edge} = \frac{(Co/(Mo + W))_{slab}}{D}, \qquad (4)$$

where D is the dispersity of the active phase calculated using the HRTEM data.

The catalysts were analyzed by HRTEM on a Tecnai G2 20 instrument equipped with a LaB6 cathode at an accelerating voltage of 200 kV. The average length of particles ($\overline{L}$) and the number of NiMo(W)S layers per stack ($\overline{N}$) were determined taking into account on the order of 400–600 particles occurring in 10–15 different areas of the catalyst surface. The dispersity (D) of active-phase particles was calculated in terms of the Kasztelan hexagonal model [38] using the following equation:

$$D = \frac{M_e + M_c}{M_T} = \frac{\sum_{t=1..t} 6n_t - 6}{\sum_{t=1..t} 3n_t^2 - 3n_t + 1}, \qquad (5)$$

where M_e is the number of Mo(W) atoms on the edges of middle crystallite CoMo(W)S, M_c is the number of Mo(W) atoms on the edges of middle crystallite CoMo(W)S, M_T is the total number of Mo(W) atoms in the middle particle of the active phase, n is the number of molybdenum atoms along one side of the MoS_2 crystallite defined by its length, and t is the total number of layers in the crystallite calculated from the HRTEM data.

The catalytic properties of the synthesized samples were examined in dibenzothiophene (0.86 wt %) hydrodesulfurization and naphthalene (3 wt %) hydrogenation reactions during the co-hydrotreating of the model mixture in toluene in the flow unit equipped with a microreactor. A steel reactor was charged with the catalyst (0.25–0.5 mm fraction, 0.2 g) diluted with carborundum at a ratio of 1 : 4. Tests were run under the following conditions: temperature, 280°C; pressure, 3 MPa; a feed space velocity, 40 h^{-1}; and H_2/feedstock = 500 nL/L. Before testing, the catalysts were activated in situ by holding with a mixture of dimethyl sulfide (2 wt % sulfur) in decane at 240°C for 10 h and at 340°C for 8 h. The products were identified by gas-liquid chromatography on a Kristall-5000 chromatograph. The steady-state activity of the test samples was observed after continuous testing for 7–10 h.

The rate constants for DBT hydrodesulfurization and naphthalene hydrogenation were determined under the assumption that these are first-order reactions and were calculated by the equations

$$k_{HDS} = -\frac{F_{DBT}}{m}\ln(1 - x_{DBT}) \text{ and}$$
$$k_{HYD} = -\frac{F_{Naft}}{m}\ln(1 - x_{Naft}), \qquad (6)$$

where k_{HDS} and k_{HYD} are the rate constants (mol/(g h)) of DBT hydrodesulfurization and naphthalene hydrogenation, respectively; x_{DBT} and x_{Naph} are the conversions (%) of DBT and naphthalene; F_{DBT} and F_{Naph} are the molar consumptions (mol/h) of reagents; and m is the catalyst weight (g).

Taking into consideration that the DBT hydrodesulfurization occurs via two routes, catalyst selectivity was estimated using Eq. (7) as the ratio between the total concentration of the products of reaction following the dibenzothiophene hydrogenation route to form

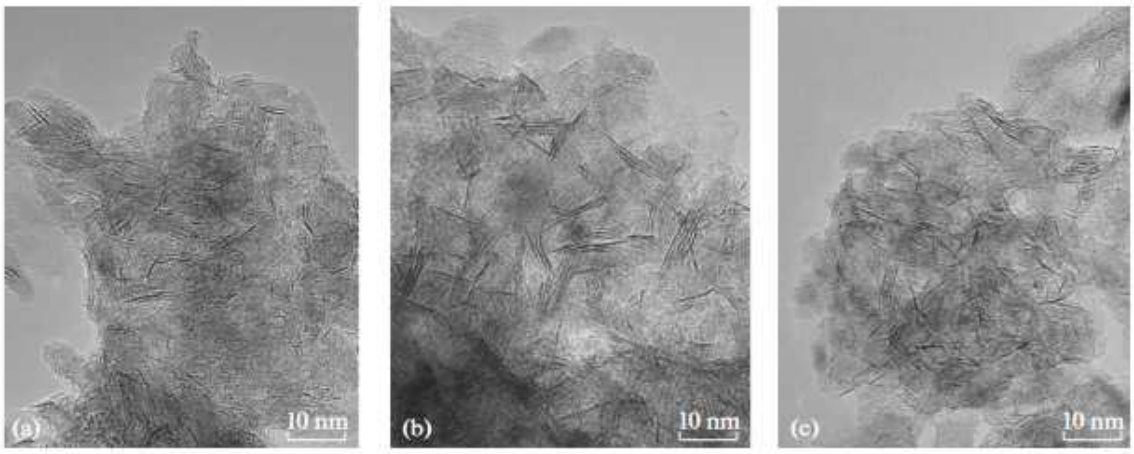

Fig. 1. TEM images of sulfided catalysts: (a) $CoMo_{12}/Al_2O_3$, (b) CoW_{12}/Al_2O_3, and (c) $CoMo_3W_9/Al_2O_3$.

tetrahydrodibenzothiophene (THDBT), bicyclohexyl (BCH), and cyclohexylbenzene (CHB) and the concentration of diphenyl (DP) formed via the direct hydrodesulfurization (DS) route:

$$S_{HYD/DS} = \frac{C_{THDBT} + C_{BCH} + C_{CHB}}{C_{DP}}, \quad (7)$$

where C_x are the concentrations of corresponding reaction products (mol %).

RESULTS AND DISCUSSION

For the test catalysts in the sulfide form, the specific surface area changed insignificantly within 265–291 m^2/g and the pore volume was ~0.50–0.55 cm^3/g. The bimodal distribution of pores with an effective diameter of 3.8 and 8.4 nm is related to coke particles formed during the sulfiding of samples containing citric acid and the effective pore size of the initial support (Table 1).

The TEM images of the sulfided catalysts are shown in Fig. 1. Black threadlike bands correspond to the layers of $Mo(W)S_2$ crystallites with a characteristic interplanar distance of about 0.65 nm [39].

The length of active-phase particles decreases in the sequence CoW_{12}/Al_2O_3 > $CoMo_{12}/Al_2O_3$ > $CoMo_3W_9/Al_2O_3$ (Table 2). The dispersity of particles varies within 0.31–0.42; the CoW_{12}/Al_2O_3 sample exhibits the minimum dispersity among the promoted catalysts.

The relative contents of Mo, W, and Co particles on the surface of sulfided $CoMo(W)/Al_2O_3$ catalysts and the degrees of promotion of $Mo(W)S_2$ crystallites according to the XPS data are summarized in Table 3. All of the catalysts possess comparable sulfiding depths. However, the content of Co in the Co(Mo)WS phase for the $CoMo_{12}/Al_2O_3$ sample was higher (0.92 wt %) compared with $CoMo_3W_9/Al_2O_3$ (0.51 wt %) and CoW_{12}/Al_2O_3 (0.26 wt %) catalysts. Probably, these results may be explained by the fact that for tungsten oxide the temperature of sulfuding is much higher than that for molybdenum and cobalt oxides [40]. As a result, for the CoW_{12}/Al_2O_3 sample, the proportion of MoS_2 is higher than that of WS_2 and the content of individual Co_9S_8 is maximal (79 rel. %). For the mixed catalyst, the selectivity for formation of the Co(Mo)WS active phase and the degree of promo-

Table 2. Morphology of active-phase particles of $CoMo(W)/Al_2O_3$ catalysts

Catalyst	Average length $\overline{L}$, nm	Average number of $Mo(W)S_2$ layers in crystallite $\overline{N}$	Dispersity of $Mo(W)S_2$ particles D[1]
$CoMo_{12}/Al_2O_3$	3.0	1.6	0.38
CoW_{12}/Al_2O_3	3.8	2.0	0.31
$CoMo_3W_9/Al_2O_3$	2.7	1.5	0.42

[1] The dispersity of $Mo(W)S_2$ particles was calculated from the HTEM data using Eq. (5).

Table 3. Content of molybdenum, tungsten, and nickel particles on the surface of sulfide $CoMo(W)/Al_2O_3$ catalysts and degree of promotion of crystallites according to the XPS data

Catalysts	Mo content, rel. %			W content, rel. %			Co content, rel. %			$C_{Co(Mo)WS}$, wt %[1]	$\left(\frac{Co}{Mo+W}\right)_{slab}$[2]	$\left(\frac{Co}{Mo+W}\right)_{edge}$[3]
	MoS_2	MoS_xO_y	Mo^{6+}	WS_2	WS_xO_y	W^{6+}	Co(Mo)WS	Co_9S_8	Co^{2+}			
$CoMo_{12}/Al_2O_3$	80	11	9	–	–	–	51	29	20	0.92	0.33	0.88
CoW_{12}/Al_2O_3	–	–	–	68	8	24	8	79	13	0.26	0.12	0.40
$CoMo_3W_9/Al_2O_3$	86	8	24	70	8	22	12	76	12	0.51	0.20	0.47

[1] Co content in the Co(Mo)WS phase was calculated from the XPS data using Eq. (2).
[2] The degree of promotion of Co/(Mo+W) particles was calculated from the XPS data through Eq. (3).
[3] The degree of promotion of Co/(Mo+W) particle edges was calculated from XPS and TEM data through Eq. 4.

Table 4. Catalytic behavior of $CoMo(W)/Al_2O_3$ catalysts in DBT hydrodesulfurization and naphthalene dehydrogenation

Catalyst	Conversion, %		Rate constants, $\times 10^4$ mol/(h g)		Selectivity $S_{HYD/DS}$
	dibenzothiophene	naphthalene	k_{HDS}	k_{HYD}	
$CoMo_{12}/Al_2O_3$	46.8	6.2	32.2	2.3	0.10
CoW_{12}/Al_2O_3	6.6	1.1	3.2	0.4	0.01
$CoMo_3W_9/Al_2O_3$	22.0	3.3	11.2 (10.5)*	1.2 (0.9)*	0.07

* The values of rate constants calculated by the additivity method are shown in parentheses.

tion of active-phase particles grow compared with CoW_{12}/Al_2O_3.

The data on the catalytic activity of the synthesized catalysts are presented in Table 4.

The conversion of reagents was varied from 6.6 to 46.8%. The lowest activity was exhibited by the CoW_{12}/Al_2O_3 catalyst in both DBT hydrodesulfurization and naphthalene hydrogenation. Among the tested catalysts the highest activity was observed for $CoMo_{12}/Al_2O_3$. The selectivity of the dibenzothiophene preliminary hydrogenation route for the tested catalysts varied within 0.01–0.10 and was lower compared with monometallic Mo_{12}/Al_2O_3 and W_{12}/Al_2O_3 catalysts (0.7 and 0.9, respectively [28]). This fact provides evidence for the generation of new promoted sites. In addition, the rates constants for HDS and HYD over the $CoMo_3W_9/Al_2O_3$ catalyst were calculated by the additivity method. The experimental value for DBT hydrodesulfurization was slightly above the calculated one (by 6%); for naphthalene hydrogenation, by 25%. The highest rates constants for DBT hydrodesulfurization and naphthalene hydrogenation were attained in the case of the $CoMo_{12}/Al_2O_3$ catalyst.

Figure 2 shows the dependence of the rate constant of dibenzothiophene hydrodesulfurization on the content of Co(Ni) in particles of the Co(Ni)(Mo)WS active phase for catalysts promoted by Co and Ni. At a comparable content of the promoter in active-phase particles on $NiMo_3W_9/Al_2O_3$ and $CoMo_3W_9/Al_2O_3$ samples, the catalyst promoted by nickel showed a higher activity. Moreover, for $(Ni)CoMo_{12}/Al_2O_3$ catalysts, activity analogous to that of Mo_3W_9/Al_2O_3 may be achieved only at a higher promoter content in the Co(Ni)(Mo)WS phase (Fig. 3). This synergism observed when Ni was used as a promoter for the mixed NiMoWS active phase is probably associated with a more optimum value of metal-sulfur binding energy (ΔE_{MS}) than that in the bimetallic samples and CoMoWS [23].

Analysis of the dependence of the rate constant of DBT hydrodesulfurization on the degree of promotion of edges of the $(Mo)WS_2$ phase (Fig. 3) makes it possible to conclude that the replacement of SiW_{12} HPA with MoW-containing $SiMo_3W_9$ HPA leads to a rise in the degree of decoration of $MoWS_2$ crystallite edges for the series of catalysts promoted by both Co and Ni. In addition, the use of Ni entails a higher degree of promotion for edges of active-phase particles compared with Co. For the $NiMo_3W_9/Al_2O_3$ catalyst, the degree of promotion is commensurable with that of $NiMo_{12}/Al_2O_3$ and $CoMo_{12}Al_2O_3$ samples. These

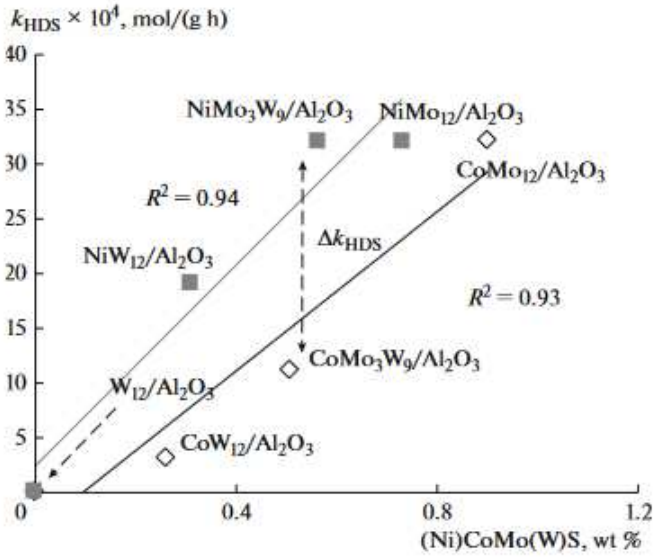

Fig. 2. Rate constant of DBT hydrodesulfurization vs. the content of Co(Ni) in particles of the Co(Ni)(Mo)WS active phase in the catalysts promoted by Co and Ni. For the series of Ni-promoted catalysts, calculated from [1]; for W_{12}/Al_2O_3, calculated from [28].

results may be attributed to the fact that the atoms of promoters (Co or Ni) are localized on different edges of tungsten sulfide: Ni on the metal edge (Me edge) or on both edges (Me and S edges), while Co predominantly inserts via the S edge [41–43]. A high degree of

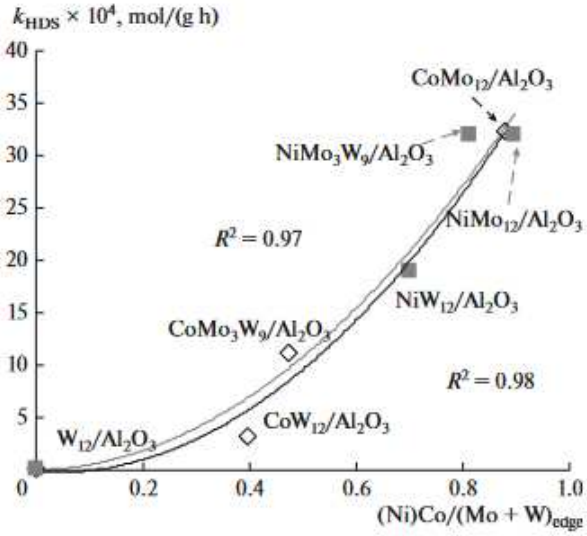

Fig. 3. Rate constant of DBT hydrodesulfurization vs. the degree of promotion of edges of Co(Ni)(Mo)WS active-phase particles in the catalysts promoted by Co and Ni. For the series of Ni-promoted catalysts, calculated from [1]; for W_{12}/Al_2O_3, calculated from [28].

Ni promotion may also be associated with the above-mentioned mechanism of post-formation of NiWS sites via the redistribution of NiS_x particles. It is evident that, in the case of nickel, the probability of relocalization on both edges will be higher than that for cobalt on the S edge. Moreover, a higher stability of the nickel complex with citric acid compared with its cobalt counterpart [44] is favorable for the synchronous formation of the promoted NiWS active phase.

Thus, the effect of Co promotion in the $CoMo_3W_9/Al_2O_3$ mixed trimetallic catalyst has been compared with $CoMo_{12}/Al_2O_3$ and CoW_{12}/Al_2O_3 catalysts, and the influence of the nature of the promoter on the physicochemical and catalytic properties of bi- and trimetallic sulfide catalysts has been explored.

It has been shown that the catalytic activity in both DBT dihydrodesulfurization and naphthalene hydrogenation decreases in the following sequence: $CoMo_{12}/Al_2O_3 > CoMo_3W_9/Al_2O_3 > CoW_{12}/Al_2O_3$, and it correlates with the degree of promotion of active-phase particles by cobalt atoms.

The general regularity which makes itself evident in that the use of mixed $H_4SiMo_3W_9O_{40}$ HPA instead of monometallic $H_4SiW_{12}O_{40}$ HPA causes an increase in the degree of decoration of edges of $MoWS_2$ crystallites for the series catalysts promoted by both Co and Ni has been established. It is shown that the use of Ni as a promoter facilitates a higher degree of promotion of edges of active-phase particles compared with Co apparently owing to differences in the stability of citrate complexes and, hence, in the rates of their sul-

fiding and different tendencies toward localization on the edges of $Mo(W)S_2$ crystallites.

The activity of bimetallic $(Ni)CoMo_{12}/Al_2O_3$ catalysts comparable with that of trimetallic $NiMo_3W_9/Al_2O_3$ samples may be achieved only at a higher content of the promoter in particles of the active phase. This synergistic effect is probably provided by the metal-sulfur binding energy (ΔE_{MS}) in NiMoWS which is more optimal for catalysis than that in bimetallic CoMoS (NiMoS) counterparts.

ACKNOWLEDGMENTS

This work was supported by the Ministry of Education and Science of the Russian Federation, project no. 14.586.21.0054 (unique project identifier RFMEFI58617X0054). This work was carried out using equipment of the Center for Collective Use Study of Physicochemical Properties of Substances and Materials, Samara State Technical University.

REFERENCES

1. M. S. Nikul'shina, A. V. Mozhaev, P. P. Minaev, M. Fournier, C. Lancelot, P. Blanchard, E. Payen, C. Lamonier, and P. A. Nikul'shin P.A., Zh. Prikl. Khim. (S.–Peterburg), No. 90, 40 (2017).
2. A. Stanislaus, A. Marafi, and M. Rana, Catal. Today **153**, 1 (2010).
3. Y. Okamoto, Bull. Chem. Soc. Jpn. **87**, 20 (2014).
4. H. Topsoe, B. S. Clausen, N. Topsoe, and E. Pederson, Ind. Eng. Chem. Fundam. **25**, 25 (1986).
5. Y. G. Hur, M.-S. Kim, D.-W. Lee, S. Kim, H.-J. Eom, G. Jeong, M.-H. No, N. S. Nho, and K.-Y. Lee, Fuel **137**, 237 (2014).
6. J. A. Tavizon-Pozos, V. A. Suarez-Toriello, J. A. Reyes, A. Guevara-Lara, B. Pawelec, J. L. G. Fierro, M. Vrinat, and C. Geantet, Topics in Catal. **59**, 241 (2016).
7. T. Alphazan, A. Bonduelle-Skrzypczak, C. Legens, Z. Boudene, A.-L. Taleb, A. -S. Gay, O. Ersen, C. Coperet, and P. Raybaud, J. Catal. **340**, 60 (2016).
8. D. D. Whitehurst, T. Isoda, and I. Mochida, Adv. Catal. **42**, 345 (1998).
9. R. Prins, V. H. J. de Beer, and G. A. Somorjai, Catal. Rev., Sci. Eng. **31**, 1 (1989).
10. S. Eijsbouts, Appl. Catal., A **158**, 53 (1997).
11. Y. Okamoto, M. Kawano, T. Kawabata, T. Kubota, and I. Hiromitsu, J. Phys. Chem. B **109**, 288 (2005).
12. F. Besenbacher, M. Brorson, B. S. Clausen, S. Helveg, B. Hinnemann, J. Kibsgaard, J. V. Lauritsen, P. G. Moses, J. K. Norskov, and H. Topsoe, Catal. Today **130**, 86 (2008).
13. M. J. Vissenberg, Y. van der Meer, E. J. M. Hensen, V. H. J. de Beer, A. M. van der Kraan, R. A. van Santen, and J. A. R. van Veen, J. Catal. **198**, 151 (2001).
14. L. Coulier, G. Kishan, J. A. R. van Veen, and J. W. Niemantsverdriet, J. Phys. Chem. B **106**, 5897 (2002).
15. R. Obeso-Estrella, J. L. G. Fierro, J. N. Diaz De Leon, S. Fuentes, G. Alonso-Nunez, E. Lugo-Medina, B. Pawelec., and T. A. Zepeda, Fuel **233**, 644 (2018).
16. R. Huirache-Acuna, B. Pawelec, E. M. Rivera-Munoz, R. Guil-Lopez, and J. L. G. Fierro, Fuel **198**, 145 (2017).
17. Y. E. Licea, R. Grau-Crespo, L. A. Palacio, and Jr. A. C. Faro, Catal. Today **292**, 84 (2017).
18. G. Kishan, L. Coulier, J. A. R. van Veen, and J. W. Niemantsverdriet, J. Catal. **200**, 194 (2001).
19. N. Rinaldi, T. Kubota, and Y. Okamoto, Appl. Catal., A **374**, 228 (2010).
20. V. M. Kogan, P. A. Nikul'shin, V. S. Dorokhov, E. A. Permyakov, A. V. Mozhaev, D. I. Ishutenko, O. L. Eliseev, N. N. Rozhdestvenskaya, and A. L. Lapidus, Izv. Akad. Nauk, Ser. Khim., No. 2, 332 (2014).
21. J. A. Mendoza-Nieto, O. Vera-Vallejo, L. Escobar-Alarcon, D. A. Solis-Casados, and T. Klimova, Fuel **110**, 268 (2013).
22. S. Sigurdson, V. Sundaramurthy, A. K. Dalai, and J. Adjaye, J. Mol. Catal. A: Chemical **291**, 30 (2008).
23. C. Tomazeau, C. Geantet, M. Lacroix, M. Danot, V. Harle, and P. Raybaud, Appl. Catal., A **322**, 92 (2007).
24. H. Yu, S. Li, and G. Jin, Energy Fuels **24**, 4419 (2010).
25. D. Liu, L. Liu, G. Li, and C. Liu, J. Nat. Gas Chem. **19**, 530 (2010).
26. R. Huirache-Acuna, B. Pawelec, E. Rivera-Munoz, R. Nava, J. Espino, and J. L. G. Fierro, Appl. Catal., B **92**, 168 (2009).
27. M. E. Cervantes-Gaxiola, M. Arroyo-Albiter, A. Perez-Larios, P. B. Balbuena, and J. Espino-Valencia, Fuel **113**, 733 (2013).
28. M. S. Nikul'shina, A. V. Mozhaev, P. P. Minaev, M. Fournier, C. Lancelot, P. Blanchard, E. Payen, C. Lamonier, and P. A. Nikul'shin, Kinet. Katal., No. 6, 789 (2017).
29. M. S. Nikulshina, A. Mozhaev, C. Lancelot, M. Marinova, P. Blanchard, E. Payen, C. Lamonier, and P. Nikulshin, Appl. Catal., B **224**, 951 (2018).
30. S. L. Amaya, G. Alonso-Nunez, T. A. Zepeda, S. Fuentes, and A. Echavarria, Appl. Catal., B 148–149, 221 (2014).
31. R. Huirache-Acuna, T. A. Zepeda, E. M. Rivera-Munoz, R. Nava, C. V. Loricera, and B. Pawelec, Fuel **149**, 149 (2015).
32. C. Rocchiccioli-Deltcheff, M. Fournier, R. Franck, and R. Thouvenot, Inorg. Chem. **22**, 207 (1983).
33. G. Herv and A. Teze, Inorg. Chem. **16**, 2115 (1977).
34. C. Sanchez, J. Livage, J. P. Launay, M. Fournier, and Y. Jeannin, J. Am. Chem. Soc. **104**, 3194 (1982).
35. A. V. Mozhaev, P. A. Nikulshin, Al. A. Pimerzin, K. I. Maslakov, and A. A. Pimerzin, Catal. Today **271**, 80 (2016).
36. P. A. Nikulshin, A. V. Mozhaev, K. I. Maslakov, A. A. Pimerzin, and V. M. Kogan, Appl. Catal., B 158–159, 161 (2014).
37. P. P. Minaev, P. A. Nikulshin, M. S. Kulikova, A. A. Pimerzin, and V. M. Kogan, Appl. Catal., A **505**, 456 (2015).

38. S. Kasztelan, H. Toulhoat, J. Grimblot, and J. P. Bonnelle, Appl. Catal. **13**, 1279 (1984)

39. H. Toulhoat and P. Raybaud, IFP Energies nouvelles **68**, 832 (2013).

40. T. Kubota, N. Miyamoto, M. Yoshioka, and Y. Okamoto, Appl. Catal., A **480**, 10 (2014).

41. M. Sun, A. E. Nelson, and J. Adjaye, J. Catal. **226**, 41 (2004).

42. H. Schweiger, P. Raybaud, and H. Toulhoat, J. Catal. **212**, 33 (2002).

43. M. Sun, A. E. Nelson, and J. Adjaye, J. Catal. **226**, 32 (2004).

44. D. Wyrzykoiwski and L. Chmuirzynski, J. Therm. Anal. Calorim. **102**, 61 (2010). J. Therm. Anal. Calorim.

Translated by T. Soboleva